Journal Pre-proofs

A zeolitic imidazolate framework with uncoordinated cyano groups in mixed matrix membranes for efficient propylene/propane separation

Guangli Yu, Ziyang Wang, Junchao Dong, Fei Ni, Dandan Song, Terence Xiaoteng Liu, Zhanhui Yuan, Kangjun Wang, Xiaoqin Zou

PII: S1385-8947(25)00151-2
DOI: https://doi.org/10.1016/j.cej.2025.159352
Reference: CEJ 159352

To appear in: *Chemical Engineering Journal*

Please cite this article as: G. Yu, Z. Wang, J. Dong, F. Ni, D. Song, T.X. Liu, Z. Yuan, K. Wang, X. Zou, A zeolitic imidazolate framework with uncoordinated cyano groups in mixed matrix membranes for efficient propylene/propane separation, *Chemical Engineering Journal* (2025), doi: https://doi.org/10.1016/j.cej.2025.159352

A zeolitic imidazolate framework with uncoordinated cyano groups in mixed matrix membranes for efficient propylene/propane separation

Guangli Yu[a,¶], Ziyang Wang[b,¶], Junchao Dong[b,¶], Fei Ni[a], Dandan Song[a], Terence Xiaoteng Liu[c,*], Zhanhui Yuan[d], Kangjun Wang[a,*], Xiaoqin Zou[b,*]

[a] College of Chemical Engineering, Shenyang University of Chemical Technology, Shenyang 110142, P. R. China

[b] Faculty of Chemistry, Northeast Normal University, Changchun 130024, P. R. China

[c] Department of Mechanical and Construction Engineering, Northumbria University, Newcastle upon Tyne NE1 8ST, United Kingdom

[d] College of Materials Engineering, Fujian Agriculture and Forestry University, Fuzhou 350002, P. R. China.

¶ These authors contributed equally to this work.

* Corresponding authors.

E-mail addresses: terence.liu@northumbria.ac.uk (T. Liu); wangkj_dut@syuct.edu.cn (K. Wang); zouxq100@nenu.edu.cn (X. Zou).

Abstract

Membrane technology is poised to substantially lower the energy consumption involved in the separation of C_3H_6 from C_3H_8. However, the quest for suitable membrane materials for this critical process remains an ongoing challenge. Herein, a novel metal-organic framework (MOF) having cyano groups, thus referring to CN-ZIF-8, has been successfully identified and developed as productive nanofillers into 6FDA-DAM polymer. Unlike ZIF-8, CN-ZIF-8 exhibits a stronger affinity for C_3H_6 and demonstrates favorable thermodynamic selectivity for recognizing it from C_3H_8 due to the presence of dangling cyano groups, as confirmed by gas sorption. The optimal membrane with a 15 wt% CN-ZIF-8 loading evinces improved separation performance in terms of ≥80% increase in ideal selectivity (~23.6) and 144% in C_3H_6 permeability (~379.8 Barrer) compared to the pristine 6FDA-DAM membrane. Mixed gas separation of a $50C_3H_6$:$50C_3H_8$ delivers remarkable separation results, out-performing the current trade-off limits associated with conventional polymer membranes. The synergistic effects of high gas solubility and the unique diffusivity behavior of CN-ZIF-8 effectively discriminate C_3H_6 from C_3H_8. This study offers valuable insights into the exploration and the design of MOFs intended for the industrial C_3H_6/C_3H_8 separation.

Keywords: Metal organic frameworks, CN-ZIF-8; Separation membranes; Thermodynamic selectivity; C_3H_6/C_3H_8 separation

1. Introduction

Propylene (C_3H_6) is an essential organic compound extensively utilized as a foundational ingredient in producing numerous plastics and polymers in the petrochemical sector [1]. In 2016, global output reached 100 million tons, with a projected annual increase of 4.0% through 2025 [2]. In general, C_3H_6 is produced primarily through the cracking of naphtha, which inevitably contains many other products, mostly propane (C_3H_8). Nevertheless, due to the subtle discrepancy in physicochemical properties between C_3H_6 and C_3H_8 (kinetic diameters: 0.4 nm *vs.* 0.42 nm and boiling points: 226 K *vs.* 231 K, respectively), the separation of C_3H_6/C_3H_8 faces a great challenge [3,4]. The current thermally-driven distillation process is extremely energy-intensive, representing approximately 0.3% of global energy consumption [5]. Accordingly, there is a continued focus in both academic and industrial research on developing alternative technologies for the C_3H_6/C_3H_8 separation that offer improved energy efficiency, smaller carbon footprint, and lower capital cost.

The membrane-based separation process, known for saving up to 90% energy than cryogenic distillation, has garnered a lot of attention for the C_3H_6/C_3H_8 separation [5]. Polymeric membranes offer a low-cost and easily processable option; however, they typically subject to the widely recognized compromise between selectivity and permeability [6-8]. Molecular sieves-based inorganic membranes can perform better separation performance; however, they face challenges in large-scale fabrication stemming from uncontrollable inter-crystalline defects [9,10]. To address these challenges, mixed matrix membranes (MMMs), which combine inorganic fillers with a polymer matrix, have been the subject of extensive research owing to their potential to leverage the benefits of both materials [11,12]. A range of fillers, including zeolites, porous organic frameworks (POFs), and metal-organic frameworks (MOFs), are being explored for gas separation applications in MMMs [13-17]. Among these, MOFs stand out due to their structures of metal ions or clusters coordinated by multidentate organic ligands, offering notable potential thanks to their chemical versatility, nanoscale porosity, and adjustable pore structures. Despite considerable efforts to utilize MOFs as fillers, only a few have been specifically identified for C_3H_6/C_3H_8 separation [18-39], with the primary emphasis on zeolitic imidazolate frameworks (ZIFs), particularly ZIF-8. Unfortunately, most of them have comparable C_3H_6/C_3H_8 equilibrium adsorption capacities due to the non-polar pore surface lacking specific interactions with C_3H_6. When these fillers are applied in the separation of C_3H_6/C_3H_8, the separation efficiency is mainly governed by variations in adsorption kinetics within MOFs that feature narrow pore structures. However, molecular sieving separations that rely on diffusion are highly sensitive to even minor

alterations (~0.1 Å) in effective pore apertures [40]. Additionally, such unfavorable thermodynamic effects may restrict the utmost separation efficiency of MOF fillers. This suggests that there remains plenty of scope to boost separation performance through the precise adjustment of pore chemistry. To this regard, this paper intends to explore efficient separation of C_3H_6/C_3H_8 through synergetic effects of thermodynamics and kinetics which are seldom reported up to date.

In this work, we customized a porous ZIF, hereafter called CN-ZIF-8, which was extensively characterized using various analytical techniques. Structurally, CN-ZIF-8 is isoreticular to the previously reported ZIF-8, inheriting its exceptional kinetic property alike molecular sieving. Notably, by intentionally introducing polar groups onto the pore walls, the adsorption behavior of C_3H_6 and C_3H_8 is significantly altered. The adsorption studies reveal that CN-ZIF-8 demonstrates a greater adsorption capacity and a stronger binding affinity for C_3H_6 compared to C_3H_8, leading to favorable thermodynamic separation of the C_3H_6/C_3H_8 mixture. Subsequently, the nanosized CN-ZIF-8 particles were embedded into a polyimide matrix 6FDA-DAM to create MMMs. These membranes were then employed for C_3H_6/C_3H_8 separation. As anticipated, the CN-ZIF-8/6FDA-DAM-15 membrane exhibits superior separation performance for both single and binary gases, exceeding the upper bound limits by a large margin. The underlying gas transport mechanisms were further clarified through the analysis of solubility and diffusion coefficients. Lastly, the impacts of feed pressure and temperature on membrane performance were systematically examined.

2. Experimental section

2.1 Chemicals

2-Methylimidazole ($C_4H_6N_2$, abbreviated as 2-MeIM, Shanghai Macklin Biochemical Co., Ltd, 98%), 4,5-dicyanoimidazole ($C_5H_2N_4$, abbreviated as DCI, Aladdin, 99%), sodium formate ($CHNaO_2$, Tianjin Hengxing Chemical Preparation Co. Ltd., AR) and dehydrated *N*-methyl-2-pyrrolidone (C_5H_9NO, Energy Chemical, 99.5%) were procured from the respective chemical companies. Analytical grade reagents including zinc nitrate hexahydrate ($Zn(NO_3)_2{\cdot}6H_2O$), chloroform ($CHCl_3$), *N,N*-dimethylformamide (DMF), methanol, triethylamine ($C_6H_{15}N$) and acetic anhydride ($C_4H_6O_3$) were acquired from local suppliers. For the synthesis of 6FDA-DAM, 4,4'-(hexafluoroisopropylidene)diphthalic anhydride (abbreviated as 6FDA, 99%) and 2,4,6-trimethyl-1,3-phenylenediamine (abbreviated as DAM, 98%) were obtained from TCI. Prior to their utilization, both 6FDA and DAM underwent purification through vacuum sublimation.

2.2 Synthesis of ZIF-8 nanocrystals

ZIF-8 was synthesized in accordance with the methodology outlined by Li *et al* [41]. Typically, $Zn(NO_3)_2{\cdot}6H_2O$ (600 mg, 2 mmol) and 2-MeIM (1320 mg, 16 mmol) were each dissolved in methanol (10 mL) and water (20 mL), respectively. The two

solutions were then combined at room temperature and stirred for a period of 10 hours. The resulting white powder was collected through centrifugation, rinsed with fresh methanol, and subsequently air-dried overnight.

2.3 Synthesis of CN-ZIF-8 nanocrystals

$Zn(NO_3)_2 \cdot 6H_2O$ (236 mg, 0.8 mmol), sodium formate (108.8 mg, 1.6 mmol) and DCI (188.8 mg, 1.6 mmol) were introduced into a 20 mL screw-capped vial. After adding DMF (8 mL) and methanol (8 mL), the mixture was subjected to ultrasonication for 10 minutes to ensure homogeneity. Thereafter, the solution was stirred at room temperature for a period of 7 days. Following crystallization, the resulting powder was centrifuged, and thoroughly rinsed with DMF. The sediment after centrifugation was soaked in methanol three times, and during this process, the methanol was replenished every 24 hours. The final product was air-dried.

2.4 Synthesis of 6FDA-DAM

The synthesis was conducted through a step-growth polymerization reaction involving 6FDA and DAM, aligned with the method outlined by Wang *et al* [42].

2.5 Fabrication of MMMs

The solution casting technique was employed to produce composite membranes. The series of MMMs were labeled as CN-ZIF-8/6FDA-DAM-X (where X = 10, 15, 20, and 25%), with X representing the mass percentage of CN-ZIF-8 incorporated into the membrane. CN-ZIF-8/6FDA-DAM-15 membrane was given as an example to illustrate the overall synthesis process. In detail, 0.5 g 6FDA-DAM was dissolved in 9.5 g (~6.4 mL) $CHCl_3$ and magnetically stirred for 4 hours to obtain a 5 wt% homogeneous solution. Similarly, 0.1 g CN-ZIF-8 was dispersed in 1.9 g (~1.3 mL) $CHCl_3$ by stirring for 4 hours and ultrasonicating for 15 minutes to obtain 5 wt% uniform dispersion. Afterward, the polymer solution was blended with the CN-ZIF-8 dispersion in a mass ratio of 17:3 and stirred overnight to yield viscous slurry. Before the casting, the resulting suspension was ultrasonicated again to remove any air bubbles. About 0.4 mL of the suspension solution was subsequently poured on a flat quartz disc. After the solvent evaporation for 10 hours under ambient atmosphere and at room temperature, the membrane was carefully removed with a small amount of deionized water and then stored in a desiccator for future uses. Other MMMs with varying loadings of CN-ZIF-8 were synthesized using the same process by adjusting the mass ratio between the polymer solution and the CN-ZIF-8 dispersion. The total concentration of CN-ZIF-8 and 6FDA-DAM in $CHCl_3$ was consistently kept at 5 wt% across all samples. For comparison, ZIF-8/6FDA-DAM-15 membrane containing 15 wt% ZIF-8 was fabricated using the same process as that of CN-ZIF-8/6FDA-DAM-15 membrane, except that CN-ZIF-8 was replaced by ZIF-8. Neat 6FDA-DAM membrane was also fabricated using identical procedures, but without CN-ZIF-8 addition and dispersion steps.

2.6 Characterizations

Comprehensive methodologies for characterizations were presented in the Supplementary Information (Test S1).

2.7 Gas separation measurements

The performance characteristics of the membrane were assessed using a custom gas separation setup. Initially, the membrane was secured within a permeation chamber and sealed using fluorocarbon O-rings. The membrane module's feed side was connected to the test gases, while the permeate side was connected to the carrier gas, with flow rates regulated by mass flow controllers. During the measurement, single and binary gases flowed as a feed stream with a flow rate of 20 mL min^{-1}. Ar was utilized as the carrier gas, maintained at a flow rate of 20 mL min^{-1}. The composition of the permeated gas transported by Ar was monitored using online gas chromatography (SCION 456GC). A steady state was established when the compositions of the permeate gases changed within an error margin of ≤5%. All permeation experiments were performed under these steady-state conditions. To ensure the result's reproducibility, all membranes were measured four times under each condition. The membrane permeability was defined as:

$$P_i = \frac{J_i \times l}{A \times \Delta p_i} \quad (1)$$

where P_i, J_i, and Δp_i are the permeability, molar flux, and the transmembrane pressure difference of component i, respectively; l and A represent the membrane thickness and effective area, respectively.

The gas selectivity (α) is defined in the form below:

$$\alpha_{i/j} = \frac{P_i}{P_j} = \frac{S_i}{S_j} \times \frac{D_i}{D_j} \quad (2)$$

where P_i and P_j represent the permeability of components i and j, while S_i and S_j denote their solubilities. Additionally, D_i and D_j are the diffusivities of the respective components i and j, respectively. The values of S_i and S_j can be determined based on gas uptakes measured at 308 K and 3 bars (C_3H_6 and C_3H_8 uptakes of 31.9 and 30.4 cm^3 g^{-1} for 6FDA-DAM, 46.1 and 28.2 cm^3 g^{-1} for CN-ZIF-8/6FDA-DAM with 15 wt% CN-ZIF-8, and 55.8 and 53.4 cm^3 g^{-1} for ZIF-8/6FDA-DAM with 15 wt% ZIF-8, respectively). The densities of 6FDA-DAM and ZIF-8 are 1.41 and 1.14, respectively [43,44]. CN-ZIF-8 and ZIF-8 are assumed to have the same density. D_i and D_j are derived from Equation (3):

$$P = S \times D \quad (3)$$

3. Results and discussion

To analyze crystal structures by single-crystal XRD, many efforts were attempted to obtain high-quality single crystals but unfortunately, all failed. Thus, we resorted to collecting powder XRD data to solve the crystallographic structure of CN-ZIF-8. As depicted in Fig. 1d, all peak positions of CN-ZIF-8 closely match those of both synthesized and simulated ZIF-8, indicative of its phase purity and high crystallinity. The pattern indexing suggests that the synthesized CN-ZIF-8 has the same three-dimensional (3D) architecture as ZIF-8; that is to say, zinc adopts a tetrahedral geometry and is 4-connected with four 4,5-dicyanoimidazole (DCI) ligands (Fig. 1a). In the DCI ligand, the 1– and 3–N atoms of imidazole ring coordinate with zinc ion and the N atom of cyano group (–CN) is unbound. Twenty-four zinc atoms and thirty-six DCI molecules are connected to generate a SOD cage, and the cages are expanded to form a 3D framework (Fig. 1b and c). FTIR spectroscopy was employed to analyze the chemical structure and functional groups. As illustrated in Fig. 1e, the absorption bands associated with Zn–N and C=N appear at 423 cm^{-1} and 1584 cm^{-1}, respectively. These findings indicate that the coordination environment in both ZIF-8 and CN-ZIF-8 remains similar, despite the incorporation of –CN into the imidazole ring. A new band at 2230 cm^{-1} originating from the stretching vibration of –CN, is observed in CN-ZIF-8, confirming the successful incorporation of DCI. Furthermore, XPS analysis reveals a comparable elemental composition for ZIF-8 and CN-ZIF-8 (Fig. S1a). Fig. S1b shows that the Zn 2p peaks observed at 1021 eV and 1044 eV are attributed to Zn $2p_{3/2}$ and Zn $2p_{1/2}$, respectively, verifying the presence of Zn–N bonds. Fig. 1f demonstrates that the binding energies of 284.8 eV, 285.9 eV, and 288.3 eV are assigned to C=C/C–C, C=N, and C–N, respectively [45]. Additionally, a signal at 286.3 eV corresponding to C≡N provides compelling evidence for the availability of DCI in CN-ZIF-8.

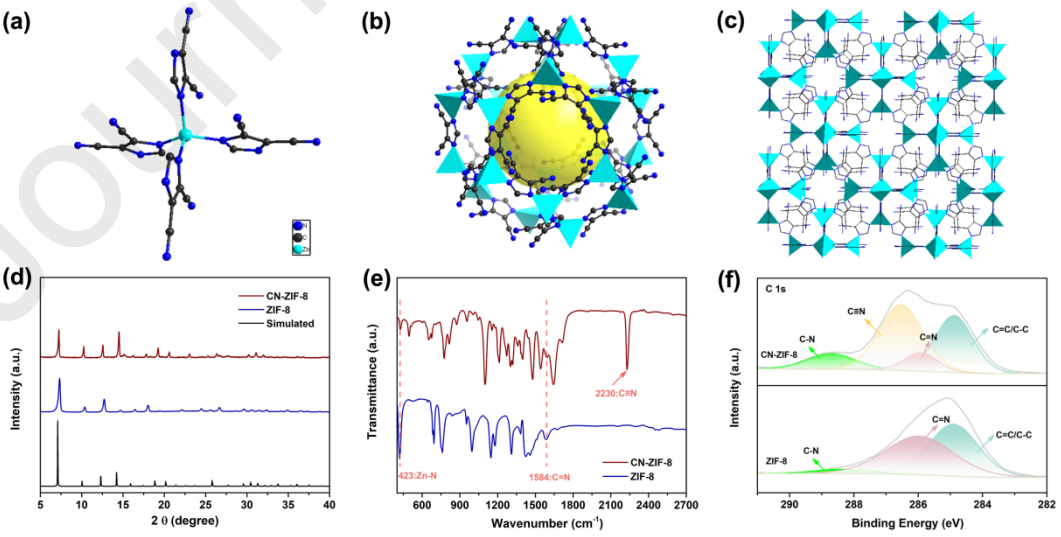

Fig. 1. (a) Coordination environments of the Zn atom in CN-ZIF-8; (b) SOD cage and (c) 3D framework of CN-ZIF-8 along the *c* axis, respectively; (d) XRD patterns simulated from ZIF-8

and collected from the synthesized ZIF-8 and CN-ZIF-8; and (e) FTIR spectra and (f) XPS C 1s spectra of ZIF-8 and CN-ZIF-8.

Gas adsorption tests were conducted to examine the porous characteristics of CN-ZIF-8. Unlike ZIF-8, the N_2 adsorption isotherm of CN-ZIF-8 at 77 K displays small N_2 uptakes at low relative pressures (Fig. S2 and Fig. 2a), a phenomenon similar to that observed in other porous nanosolids [46,47]. A rational explanation is that the molecules with dipole or quadrupole moments suffer from quadrupolar interactions in the electrostatic-field gradients near pore surfaces. Such interactions between N_2 molecules and the pores block N_2 diffusion into CN-ZIF-8, leading to a restricted adsorption behavior. In contrast, the adsorption capacity of CN-ZIF-8 for CO_2 at 195 K is notably higher. Polar –CN groups improve the interaction of CO_2 with the framework, effectively overcoming quadrupolar interactions and allowing CO_2 to enter the pores. To further investigate the porosity, CO_2 adsorption isotherms were analyzed at both 195 K and 273 K. The isotherms exhibit a pronounced uptake at $P/P_0 < 0.1$ (Fig. 2a), which is indicative of a microporous structure. Furthermore, the Brunauer-Emmett-Teller (BET) surface area is determined to be 182 m^2 g^{-1} (Fig. S3), with an estimated pore diameter of around 0.9 nm (Fig. 2b).

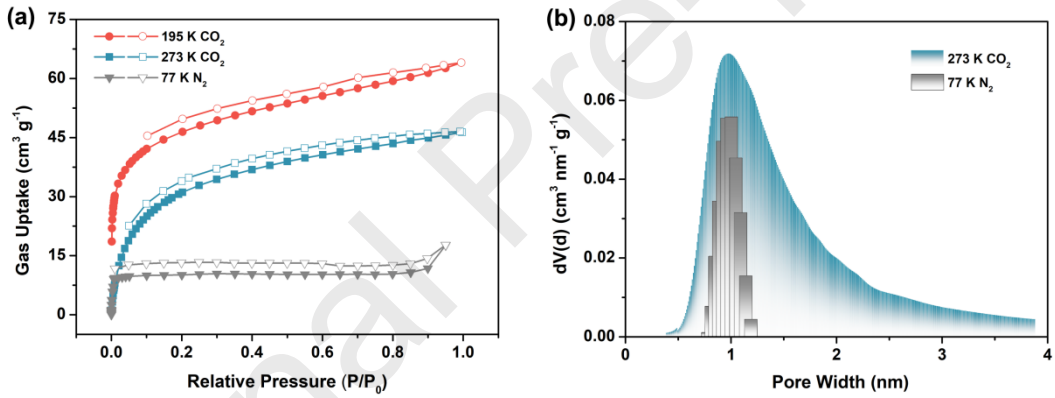

Fig. 2. (a) Adsorption isotherms of N_2 (77 K), and CO_2 (273 K and 195 K) on CN-ZIF-8, P_0 is 1.0 bar; and (b) the pore size distributions derived from both N_2 isotherm at 77 K (DFT method) and CO_2 isotherm at 273 K (SF method).

Based on its porous and cyano-rich structure, the gas adsorption properties of CN-ZIF-8 were studied. Adsorption isotherms for C_3H_6 and C_3H_8 were determined at temperatures of 298 K and 308 K, with pressures reaching up to 101 kPa. As illustrated in Fig. 3a, the C_3H_6 adsorption isotherms display a steep increase at low pressures, achieving an uptake of 43.7 cm^3 g^{-1} at 298 K and 101 kPa. In comparison, a lower uptake of 38.8 cm^3 g^{-1} for C_3H_8 is observed under the same conditions. The larger uptake for C_3H_6 by CN-ZIF-8 contrasts with the nearly equal adsorption of C_3H_6 to C_3H_8 as seen in ZIF-8 (Fig. S4) [39,48]. The favored adsorption of C_3H_6 is related to the uncoordinated –CN groups, as the C=C bond in C_3H_6 exhibits stronger acidity compared to the single C–C bond in C_3H_8 [49,50]. The highly polar –CN

groups within CN-ZIF-8 act as H-bond acceptors, significantly enhancing C_3H_6 capacity and strengthening host-guest interactions.

To quantify adsorption affinity, the isosteric heats of adsorption (Q_{st}) of CN-ZIF-8 were derived from the isotherms at 298 K and 308 K using the Virial equation. Fig. 3b demonstrates that at zero coverage, the Q_{st} value for C_3H_6 (49.1 kJ mol^{-1}) is significantly higher compared to C_3H_8 (38.7 kJ mol^{-1}). This observation reflects a stronger preference for C_3H_6 adsorption, which is in line with the adsorption isotherms. Additionally, C_3H_6 Q_{st} of CN-ZIF-8 even exceeds those of some MOFs, such as $Cu_3(BTC)_2$ (41.8 kJ mol^{-1}) [51], Fe_2(dobdc) (44 kJ mol^{-1}) [52], and GeFSIX-3-Co (42 kJ mol^{-1}) [53]. The adsorption selectivity for C_3H_6/C_3H_8 is 7.5 at 298 K under 101 kPa, as calculated by the ideal adsorbed solution theory (IAST) (Fig. 3c). These gas adsorption studies reveal that CN-ZIF-8 has a thermodynamic favorability for C_3H_6.

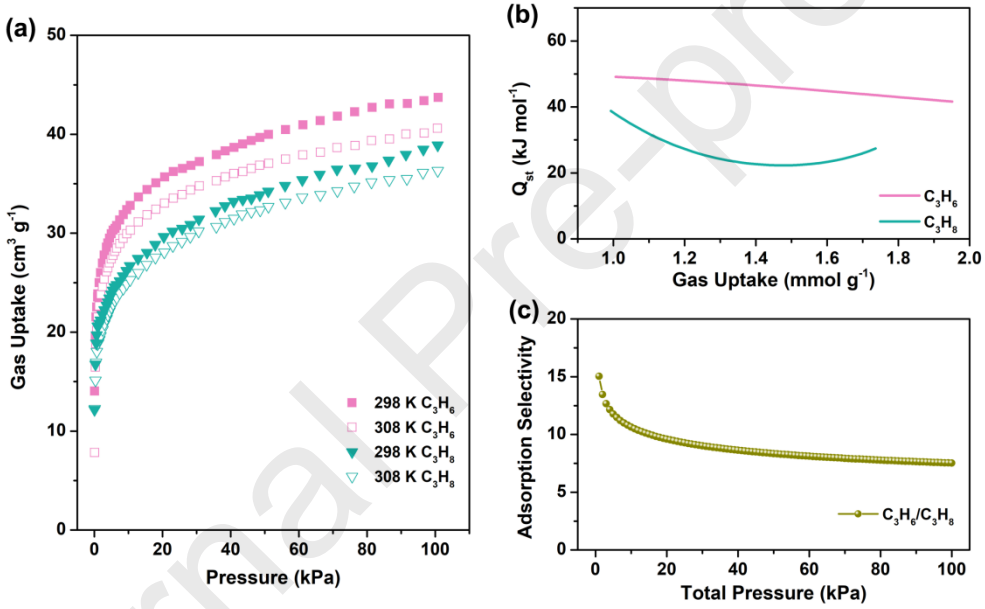

Fig. 3. (a) C_3H_6 and C_3H_8 adsorption isotherms at 298 K and 308 K; (b) Q_{st} of C_3H_6 and C_3H_8; and (c) IAST predicted selectivity for 50:50 C_3H_6/C_3H_8 binary gas mixture on CN-ZIF-8 at 298 K.

The morphology and dimension of CN-ZIF-8 were visualized by SEM. As illustrated in Fig. 4c, CN-ZIF-8 appears a quasi-spherical shape and demonstrates a high degree of uniformity. Statistical analysis of over 200 particles indicates that the average size of CN-ZIF-8 is estimated to range from 140 to 240 nm, as depicted in the histogram inset in Fig. 4c. Nanosized particles are well identified as good fillers for fabricating crack-free MMMs [54]. For 6FDA-DAM, FTIR and GPC results explicate that 6FDA-DAM is formed by chemically linked monomers (Fig. S5) and it has a macromolecular nature of good solubility in organic solvents (Fig. S6). The molecular weight (M_w) of 6FDA-DAM is 88,364 g mol^{-1}, which is considerably lower than the values (>200,000 g mol^{-1}) reported in the literature [27,55]. Previous studies indicate that a lower molecular weight enhances the mobility of polymer chains [56-58]. This

increased mobility likely results in a less densely packed structure, thereby reducing the gas-permeation resistance. The synthesized CN-ZIF-8 nanoparticles were subsequently blended with 6FDA-DAM to fabricate MMMs, and detailed microstructures of the membranes were inspected by XRD, FT-IR, TGA, SEM, and DSC measurements. For XRD patterns in Fig. 4a, the pure 6FDA-DAM membrane is amorphous structure with a broad peak at approximately 14.1°. Upon the incorporation of CN-ZIF-8 into the 6FDA-DAM matrix, characteristic diffractions associated with CN-ZIF-8 become evident. The diffraction intensity progressively increases as the loading amount of CN-ZIF-8 is elevated from 10 to 25 wt.%, reflecting a corresponding rise in porosity by the CN-ZIF-8 filler. The FT-IR spectra indicate that the bands at 423 cm^{-1} and 2230 cm^{-1} are associated with the stretching vibrations of Zn–N and –CN bonds in CN-ZIF-8, respectively. Additionally, the bands at 1720 cm^{-1} and 1786 cm^{-1} correspond to the C=O groups in 6FDA-DAM (Fig. 4b). These evidences show that the crystallinity of the embedded CN-ZIF-8 remains unaffected during the membrane fabrication process. TGA results demonstrate that the prepared MMMs with different CN-ZIF-8 loadings exhibit analogous profiles of thermal weight loss (Fig. S7). The initial stage, occurring at temperature below ~100 ℃, is ascribed to the evaporation of solvent. The second stage, which takes place between 210 ℃ and 420 ℃, is primarily due to the crystal skeleton's breakdown. The third stage, which occurs at temperature above 420 ℃, is related to the decomposition of the polymer backbones.

The cross-sectional SEM images of the 6FDA-DAM membrane display a uniform and reticular structure, as shown in Fig. S8. When the loading of CN-ZIF-8 reaches 10% or 15%, the nanoparticles are well wrapped by the 6FDA-DAM matrix without any agglomeration or visible defects (Fig. S8, Fig. 4). The EDS mapping offers additional confirmation of phase compatibility in the membrane of CN-ZIF-8/6FDA-DAM-15. Referring to Fig. 4g, the signal of Zn element solely from CN-ZIF-8 is detected uniformly, while the signals of N and C are also homogeneously disseminated because of their presences in both MOF and polymer matrix, proving the exceptional interfacial adhesion. However, upon increasing the loading of CN-ZIF-8 to 20% or 25%, a noticeable agglomeration of CN-ZIF-8 particles is observed, as shown in Fig. S8. The interfacial interactions were further explored by DSC measurements. As shown in Fig. S9, the glass transition temperature (Tg) of the pure 6FDA-DAM membrane is recorded as 366.2 ℃. Notably, with an increase in the CN-ZIF-8 loading, the Tg values of all MMMs exhibit a shift towards higher temperature. This observation implies that the mobility of the polymer chains is constrained due to effective interfacial interactions between CN-ZIF-8 and 6FDA-DAM.

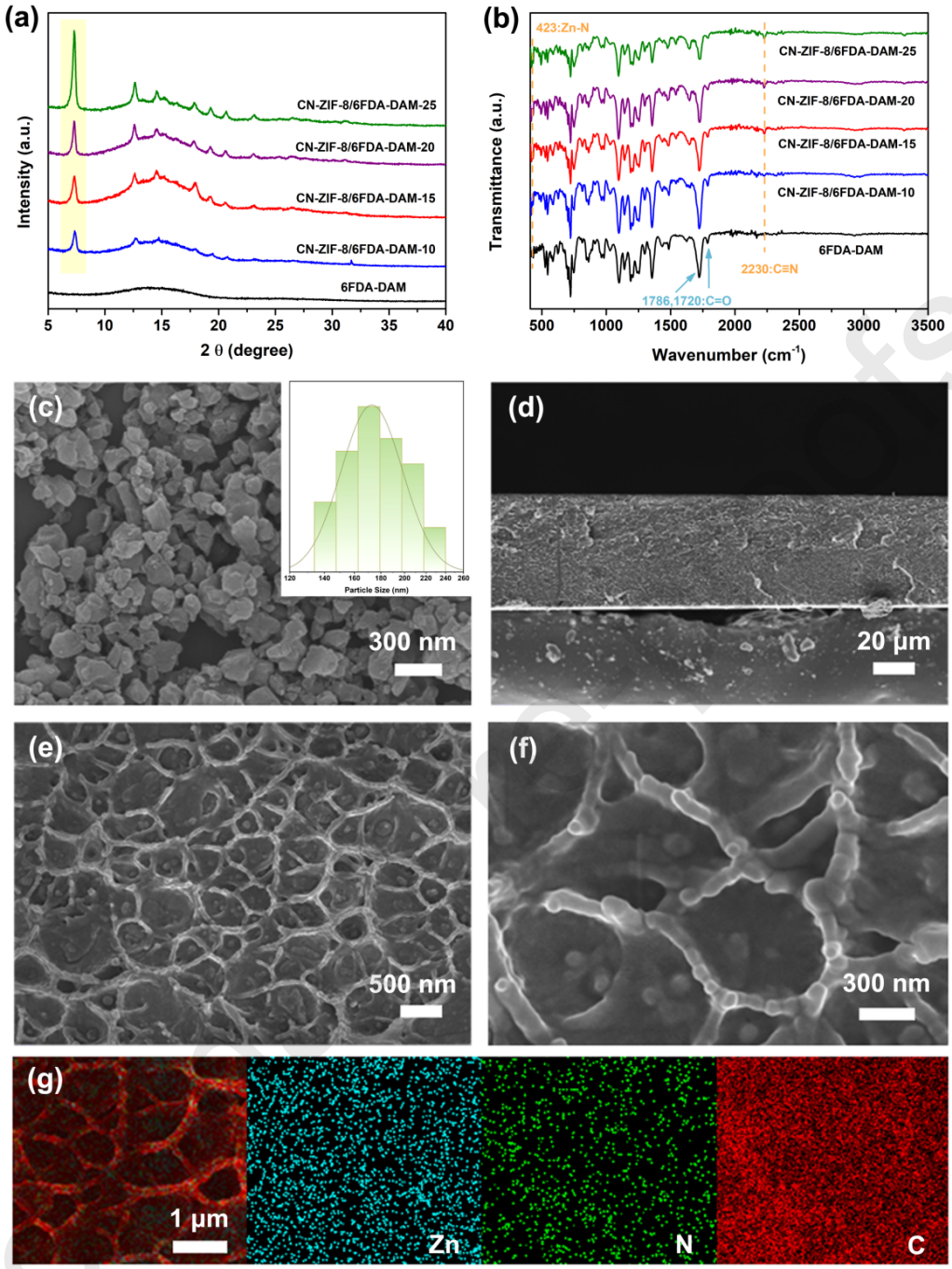

Fig. 4. (a) XRD patterns and (b) FT-IR spectra of pristine 6FDA-DAM membrane and CN-ZIF-8/6FDA-DAM MMMs with different CN-ZIF-8 loadings; (c) SEM image of CN-ZIF-8 nanoparticles and particle size distribution (inserted histogram); (d-f) cross-sectional SEM images of CN-ZIF-8/6FDA-DAM-15 membrane at various magnifications; (g) EDS mapping of Zn, N, and C elements of CN-ZIF-8/6FDA-DAM-15 membrane.

Single gas permeation characteristics of C_3H_6/C_3H_8 were initially evaluated on the CN-ZIF-8/6FDA-DAM MMMs containing 15 wt% CN-ZIF-8. ZIF-8/6FDA-DAM-15 membrane (15 wt% ZIF-8) and pristine 6FDA-DAM membrane were also conducted for comparison. As presented in Fig. 5a, the CN-ZIF-8/6FDA-DAM-15 membrane

demonstrates a C_3H_6 permeability of 379.8 Barrer and a C_3H_6/C_3H_8 selectivity of 23.6. This ideal selectivity greatly surpasses the selectivity derived from the Knudsen constant (~1.02). Moreover, the improved selectivity forcefully reinforces the assertion that the membranes are free of defects, which aligns with the findings from the SEM observations. Notably, C_3H_6 permeability and C_3H_6/C_3H_8 selectivity of CN-ZIF-8/6FDA-DAM membrane are 2.4 and 1.8 times of 6FDA-DAM, and 1.2 and 1.5 times of ZIF-8/6FDA-DAM-15 membrane, respectively. To better understand the separation mechanism, we analyzed the solubility coefficients (S) and the diffusivity coefficients (D) of the two gases within each membrane (Fig. 5b). As expected, the enhanced C_3H_6 permeability in the ZIF-8/6FDA-DAM-15 membrane can be attributed to the raise in both gas solubility and diffusivity. Conversely, the increased overall selectivity of C_3H_6/C_3H_8 only stems from the striking raise in diffusion selectivity, indicating that the diffusion selectivity of C_3H_6/C_3H_8 (D_{C3H6}/S_{C3H8}) is fully dependent on the intrinsic molecular-sieving property of ZIF-8. For the CN-ZIF-8/6FDA-DAM-15 membrane, a decrease in the solubility coefficient of C_3H_8 is observed, accompanied by a marked increase in the solubility coefficient of C_3H_6, facilitating its rapid transport. The solution selectivity of C_3H_6/C_3H_8 (S_{C3H6}/S_{C3H8}) soars approximately 1.6 times, from 1.04 for ZIF-8/6FDA-DAM-15 to 1.64 for CN-ZIF-8/6FDA-DAM-15 (Fig. 5c). This finding effectively supports the hypothesis that –CN groups enhance the selective separation of C_3H_6/C_3H_8 by favoring the adsorption of C_3H_6 within CN-ZIF-8. Concurrently, the diffusion coefficients for both C_3H_6 and C_3H_8 in the CN-ZIF-8/6FDA-DAM-15 membrane exceed those in 6FDA-DAM membrane, which aligns well with the lower diffusion resistance in porous MOFs. The diffusivity coefficient for C_3H_6 rises more dramatically than that for C_3H_8, leading to a higher D_{C3H6}/D_{C3H8}. This observation unequivocally validates the kinetic separation capability of CN-ZIF-8, attributed to the fact that CN-ZIF-8 has a comparable pore opening of 0.44 nm [59] to C_3H_6 (0.4 nm) and C_3H_8 (0.42 nm). C_3H_6 molecules diffuse faster compared to C_3H_8 molecules within these MOF pores. Taken together, it can be inferred that the abundant –CN sites and the small window contribute to favorable host-guest interactions and tunable diffusion behavior [60]. This synergy results in thermodynamic-kinetic effects that enable the efficient separation of C_3H_6/C_3H_8 in CN-ZIF-8.

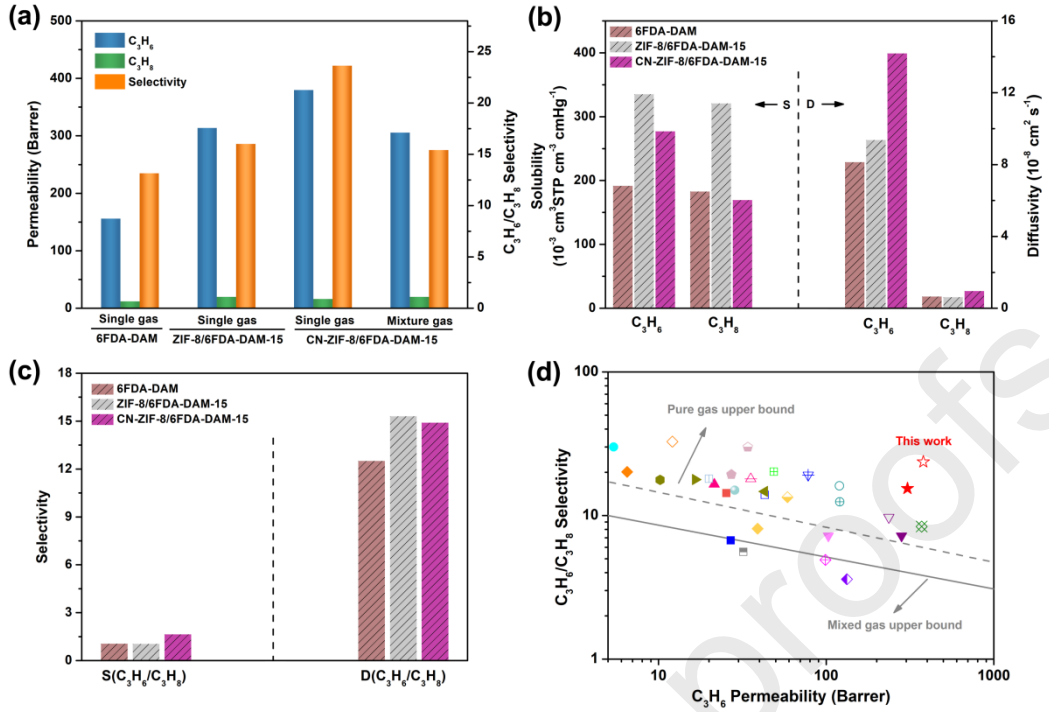

Fig. 5. (a) Separation performance of 6FDA-DAM, ZIF-8/6FDA-DAM-15 and CN-ZIF-8/6FDA-DAM-15 membranes; (b) solution and diffusivity coefficients; (c) solubility and diffusivity selectivity of 6FDA-DAM, ZIF-8/6FDA-DAM-15 and CN-ZIF-8/6FDA-DAM-15 membranes; (d) performance comparison against the Robeson upper bound and previously reported MOF-based MMMs (open for pure gas, full for mixed gas).

During binary gas permeation, the C_3H_6 permeability and C_3H_6/C_3H_8 selectivity of the CN-ZIF-8/6FDA-DAM-15 membrane are depreciated with a comparison to the single gas results (Fig. 5a). This phenomenon can be ascribed to the competition effect between C_3H_6 and C_3H_8 within the membrane, alongside the bulk effect induced by C_3H_6 [27,55]. Given the narrow pores of CN-ZIF-8, the adsorption of C_3H_8 partially blocks the diffusion pathways available for C_3H_6, leading to a decrease in C_3H_6 permeability relative to that observed under single-gas conditions. Conversely, the permeability of C_3H_8 exhibits a modest increase as a result of the polymer swelling induced by the adsorbed C_3H_6, which aids the mobility of less adsorbable C_3H_8 within the membrane. Consequently, the selectivity is somewhat lower than the ideal value. The separation performance of the CN-ZIF-8/6FDA-DAM-15 membrane was compared to other membranes documented in the literature. As plotted in Fig. 5d, the selectivity-permeability products for both single and binary gases clearly outclass the upper bound limits of polymeric membranes, positioning them in the upper-right corner and underscoring the outstanding performance of the prepared MMMs. Furthermore, these membranes also outperform most typical ZIF-based MMMs [19-21,23-36], validating that the introduction of –CN functionality is effective in directing the development of high-performance MMMs.

Fig. 6a depicts the separation performance of a mixture of C_3H_6 and C_3H_8 in MMMs with varying CN-ZIF-8 loadings, ranging from 0 wt% to 25 wt%. The C_3H_6 permeability of pristine 6FDA-DAM membrane appears to be higher than the values reported in other works [27,55], probably attributed to its lower molecular weight. With increasing CN-ZIF-8 loading, the gas permeability of the CN-ZIF-8/6FDA-DAM membrane rises steadily, while the C_3H_6/C_3H_8 selectivity initially enhances before declining. At a loading of 15 wt% CN-ZIF-8, the permeability of C_3H_8 exhibits a moderate increase from 7.0 to 19.8 Barrer. In contrast, the C_3H_6 permeability increases in larger amplitude from 79.9 to 305.4 Barrer, thereby enhancing the separation performance of C_3H_6/C_3H_8. The optimal CN-ZIF-8/6FDA-DAM-15 membrane shows C_3H_6 permeability and selectivity that are 282% and 35% higher than the pristine 6FDA-DAM membrane, respectively. This improvement is attributed to the distinct physical and chemical properties of CN-ZIF-8, which offers open size-selective pores that act as direct pathways for gas molecules. Additionally, CN-ZIF-8's strong affinity for C_3H_6 strengthens C_3H_6 solubility, thereby facilitating its selective transport. Once the CN-ZIF-8 loading exceeds 15 wt%, C_3H_6/C_3H_8 selectivity starts to decrease due to non-selective interfacial voids formed by clustering of excess CN-ZIF-8 fillers, as illustrated in SEM images (Fig. S8).

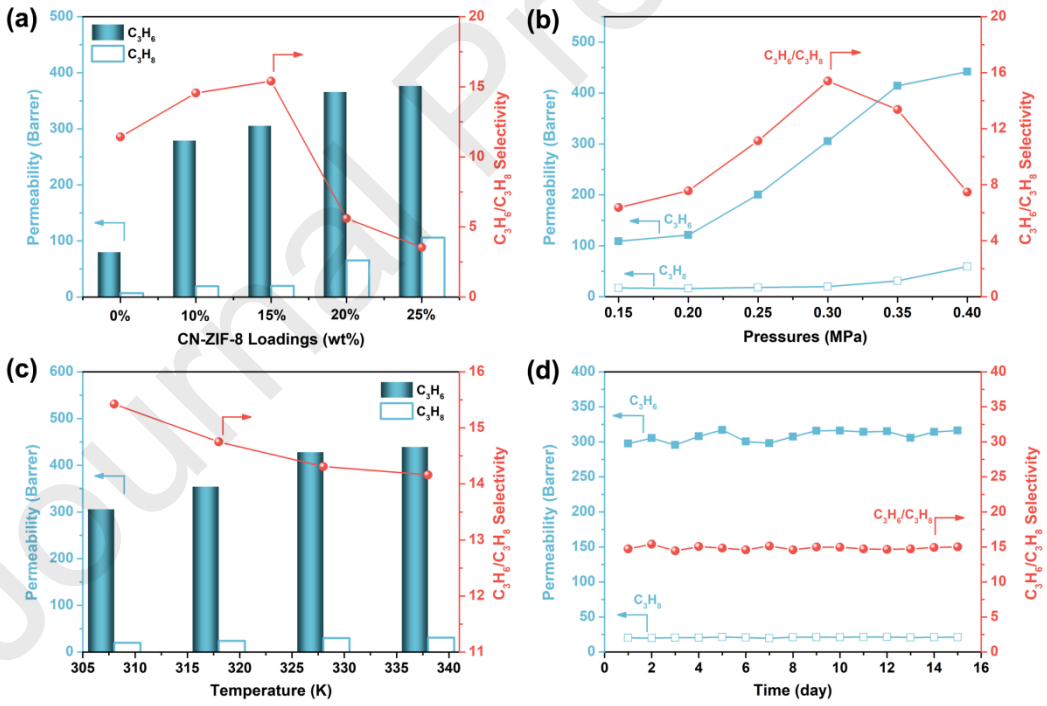

Fig. 6. (a) Permeability of C_3H_6 and C_3H_8, and the C_3H_6/C_3H_8 selectivity for the synthesized CN-ZIF-8/6FDA-DAM MMMs with varying CN-ZIF-8 loadings (0.3 MPa, 308 K, C_3H_6/C_3H_8: 50/50); C_3H_6/C_3H_8 separation performance of CN-ZIF-8/6FDA-DAM-15 membrane (b) with transmembrane pressure drops from 0.15 to 0.4 MPa (308 K, C_3H_6/C_3H_8: 50/50), (c) under operating temperatures ranging from 308 K to 338 K (0.3 MPa, C_3H_6/C_3H_8: 50/50), and (d) during a long-term stability test (0.3 MPa, 308 K, C_3H_6/C_3H_8: 50/50).

The influence of feed pressure on the CN-ZIF-8/6FDA-DAM-15 membrane's separation performance was examined, as illustrated in Fig. 6b. The C_3H_6/C_3H_8 selectivity shows volcanic shape with increasing the feed pressure, which can be explained in the following [55,61]: below 0.3 MPa, the gas transport is governed by CN-ZIF-8, namely the contribution of the MOF is dominant. As we know, CN-ZIF-8 is selective for both adsorption and diffusion for C_3H_6. The MOF contribution becomes more evident via forcing gas transport in the pores by the pressure. With elevating the pressure to 0.35 MPa, the plasticization of the membrane occurs, causing a selectivity decline. The C_3H_6 permeability increases from 108.9 to 305.4 Barrer in the pressure range of 0.15 - 0.30 MPa, and then increases to 441.8 Barrer at 0.40 MPa. At low pressure, an increase of the solubility is more than a decrease of the diffusivity [62]. This compensation leads to an increase of the permeability until maximization of solubility effect (0.30 MPa). At high pressure, the plasticization allows more and faster gas transport in the polymer of 6FDA-DAM than in the MOF of CN-ZIF-8, which also leads to a rise in gas permeability [63].

The thermal behavior of the CN-ZIF-8/6FDA-DAM-15 membrane was assessed through gas permeation tests at different temperatures, with the results plotted in Fig. 6c. The C_3H_6 permeability increases from 305.4 Barrer at 308 K to 439.0 Barrer at 338 K, representing a rise of 43.7%. Correspondingly, the C_3H_8 permeability rises by 56.6% under the same conditions. A comparable trend is noted in the ZIF-8/6FDA-DAM-15 membrane, as seen in Fig. S10. The temperature's effect on permeability can be explained by the fact that the gas diffusion coefficient increases with temperature. Additionally, temperature-induced changes in the membrane's microstructure may promote the mobility of polymer chains, thereby creating additional transport pathways for gas diffusion. At elevated temperatures, larger gas molecules (C_3H_8) exhibit greater diffusivity than smaller molecules (C_3H_6), which accounts for the decay in C_3H_6/C_3H_8 selectivity. The Arrhenius formula elucidates this trend, which posits that gas permeability increases with temperature. On the other hand, the apparent activation energies for C_3H_6 in both CN-ZIF-8/6FDA-DAM-15 (11.1 kJ mol^{-1}) and ZIF-8/6FDA-DAM-15 membranes (13.5 kJ mol^{-1}) are lower than those for C_3H_8 of 13.6 kJ mol^{-1} and 26.6 kJ mol^{-1}, respectively (Fig. S11, Fig. S12). This observation suggests that C_3H_8 is more sensitive to temperature. Despite the adverse impact of increased temperature on selectivity, the CN-ZIF-8/6FDA-DAM-15 membrane still maintains a commendable selectivity of 14.2 at 338 K, which surpasses that of ZIF-8/6FDA-DAM-15 membrane (9.2), ascribing to the affinity of polar –CN groups for C_3H_6. To investigate the stability, long-term testing was performed by exposing the CN-ZIF-8/6FDA-DAM-15 membrane to a continuous flow of a C_3H_6/C_3H_8 mixture for 15 days. Fig. 6d shows that the membrane maintains consistent performance, with a C_3H_6 permeability of around 308.5 Barrer and a C_3H_6/C_3H_8 selectivity of 15, reflecting excellent operational stability.

4. Conclusion

This study presented a novel type of MMM with cyano-ligand functionalized CN-ZIF-8 fillers, aimed at improving the separation performance for C_3H_6/C_3H_8. Characterization results revealed that the strong affinity for C_3H_6 was stemmed from the plentiful open cyano sites within the CN-ZIF-8 framework, which enhanced the adsorption capacity and selectivity for C_3H_6 over C_3H_8. As a result, the optimized MMMs achieved a C_3H_6 permeability of 379.8 Barrer, 144% higher than the 6FDA-DAM membrane, and an ideal selectivity of 23.6, an 80% improvement that exceeded the traditional trade-off limitation. Detailed solubility and diffusivity analyses provided insights into the gas transport mechanisms within the MMMs. Furthermore, the novel membrane exhibited exceptional mixed-gas separation performance and remarkable long-term stability, highlighting its potential for industrial applications in C_3H_6/C_3H_8 separation.

CRediT authorship contribution statement

Guangli Yu: Investigation, Formal analysis, Writing – original draft. **Ziyang Wang:** Investigation, Data curation, Methodology. **Junchao Dong:** Investigation, Visualization, Data curation. **Fei Ni:** Software, Visualization, Data curation. **Dandan Song:** Formal analysis. **Terence Xiaoteng Liu:** Resources, Writing – review and editing. **Zhanhui Yuan:** Resources. **Kangjun Wang:** Resources, Writing – review and editing. **Xiaoqin Zou:** Supervision, Project administration, Writing – review and editing.

Declaration of competing interest

The authors declare that they have no known competing financial interests or personal relationships that could have appeared to influence the work reported in this paper.

Data availability

Data will be made available on request.

Acknowledgments

This work was endorsed by the National Key Research and Development Program of China (2024YFE0210200), the National Natural Science Foundation of China (22208224, 22375031), the Shenyang Young and Middle-aged Science & Technology Talents Program (RC230652), the Jilin Natural Science Fund for Excellent Young Scholars (20230508116RC), the Fundamental Research Funds for the Central Universities (2412023YQ001), the Natural Science Foundation of Liaoning Province (2022-BS-213), the Excellent Youth Lift Plan from Shenyang University of Chemical

Technology (2022YQ003), and the Open Project of State Key Laboratory of Inorganic Synthesis & Preparative Chemistry, Jilin University (2023-17).

References

[1] Y.-L. Peng, C. He, T. Pham, T. Wang, P. Li, R. Krishna, K.A. Forrest, A. Hogan, S. Suepaul, B. Space, M. Fang, Y. Chen, M.J. Zaworotko, J. Li, L. Li, Z. Zhang, P. Cheng, B. Chen, Robust microporous metal-organic frameworks for highly efficient and simultaneous removal of propyne and propadiene from propylene, Angew. Chem. Int. Ed. 58 (2019) 10209-10214. https://doi.org/https://doi.org/10.1002/anie.201904312.

[2] N. Nakayama, Global Supply and Demand of Petrochemical Products Relied on LPG as Feedstock, International LP Gas Seminar: Tokyo, Japan, 2017.

[3] S. Zhou, Y. Wei, L. Li, Y. Duan, Q. Hou, L. Zhang, L.-X. Ding, J. Xue, H. Wang, J. Caro, Paralyzed membrane: current-driven synthesis of a metal-organic framework with sharpened propene/propane separation, Sci. Adv. 4 (2018) eaau1393. https://doi.org/10.1126/sciadv.aau1393.

[4] J. Gao, Y. Cai, X. Qian, P. Liu, H. Wu, W. Zhou, D.-X. Liu, L. Li, R.-B. Lin, B. Chen, A microporous hydrogen-bonded organic framework for the efficient capture and purification of propylene, Angew. Chem. Int. Ed. 133 (2021) 2-9. https://doi.org/https://doi.org/10.1002/anie.202106665.

[5] D.S. Sholl, R.P. Lively, Seven chemical separations to change the world, Nature 532 (2016) 435-437. https://doi.org/10.1038/532435a.

[6] L.M. Robeson, Correlation of separation factor versus permeability for polymeric membranes, J. Membr. Sci. 62 (1991) 165-185. https://doi.org/https://doi.org/10.1016/0376-7388(91)80060-J.

[7] L.M. Robeson, The upper bound revisited, J. Membr. Sci. 320 (2008) 390-400. https://doi.org/https://doi.org/10.1016/j.memsci.2008.04.030.

[8] R.L. Burns, W.J. Koros, Defining the challenges for C_3H_6/C_3H_8 separation using polymeric membranes, J. Membr. Sci. 211 (2003) 299-309. https://doi.org/https://doi.org/10.1016/S0376-7388(02)00430-1.

[9] K. Celebi, J. Buchheim, R.M. Wyss, A. Droudian, P. Gasser, I. Shorubalko, J.-I. Kye, C. Lee, H.G. Park, Ultimate permeation across atomically thin porous graphene, Science 344 (2014) 289-292. https://doi.org/10.1126/science.1249097.

[10] Y. Peng, Y. Li, Y. Ban, H. Jin, W. Jiao, X. Liu, W. Yang, Metal-organic framework nanosheets as building blocks for molecular sieving membranes, Science 346 (2014) 1356-1359. https://doi.org/10.1126/science.1254227.

[11] W.J. Koros, C. Zhang, Materials for next-generation molecularly selective synthetic membranes, Nat. Mater. 16 (2017) 289-297. https://doi.org/10.1038/nmat4805.

[12] G. Yu, X. Zou, L. Sun, B. Liu, Z. Wang, P. Zhang, G. Zhu, Constructing connected paths between UiO-66 and PIM-1 to improve membrane CO_2 separation with crystal-like gas selectivity, Adv. Mater. 31 (2019) 1806853. https://doi.org/https://doi.org/10.1002/adma.201806853.

[13] Y. Cheng, Y. Ying, S. Japip, S.-D. Jiang, T.-S. Chung, S. Zhang, D. Zhao, Advanced porous materials in mixed matrix membranes, Adv. Mater. 30 (2018) 1802401. https://doi.org/https://doi.org/10.1002/adma.201802401.

[14] G. Yu, H. Rong, X. Zou, G. Zhu, Engineering microporous organic framework membranes for CO_2 separations, Mol. Syst. Des. Eng. 2 (2017) 182-190. https://doi.org/10.1039/C7ME00017K.

[15] S.H. Goh, H.S. Lau, W.F. Yong, Metal-organic frameworks (MOFs)-based mixed matrix membranes (MMMs) for gas separation: a review on advanced materials in harsh environmental applications, Small 18 (2022) 2107536. https://doi.org/https://doi.org/10.1002/smll.202107536.

[16] M. Vinoba, M. Bhagiyalakshmi, Y. Alqaheem, A.A. Alomair, A. Pérez, M.S. Rana, Recent progress of fillers in mixed matrix membranes for CO_2 separation: A review, Sep. Purif. Technol. 188 (2017) 431-450. https://doi.org/https://doi.org/10.1016/j.seppur.2017.07.051.

[17] A. Knebel, J. Caro, Metal-organic frameworks and covalent organic frameworks as disruptive membrane materials for energy-efficient gas separation, Nature Nanotech. 17 (2022) 911-923. https://doi.org/10.1038/s41565-022-01168-3.

[18] Q. Shen, S. Cong, R. He, Z. Wang, Y. Jin, H. Li, X. Cao, J. Wang, B. Van der Bruggen, Y. Zhang, SIFSIX-3-Zn/PIM-1 mixed matrix membranes with enhanced permeability for propylene/propane separation, J. Membr. Sci. 588 (2019) 117201. https://doi.org/https://doi.org/10.1016/j.memsci.2019.117201.

[19] T.H. Lee, B.K. Lee, C. Youn, J.H. Kang, Y.J. Kim, K.I. Kim, Y.R. Ha, Y. Han, H.B. Park, Interface engineering in MOF/crosslinked polyimide mixed matrix membranes for enhanced propylene/propane separation performance and plasticization resistance, J. Membr. Sci. 667 (2023) 121182. https://doi.org/https://doi.org/10.1016/j.memsci.2022.121182.

[20] T.H. Lee, J.G. Jung, Y.J. Kim, J.S. Roh, H.W. Yoon, B.S. Ghanem, H.W. Kim, Y.H. Cho, I. Pinnau, H.B. Park, Defect engineering in metal-organic frameworks towards advanced mixed matrix membranes for efficient propylene/propane separation, Angew. Chem. Int. Ed. 60 (2021) 13081-13088.

https://doi.org/https://doi.org/10.1002/anie.202100841.

[21] Y. Liu, Z. Chen, G. Liu, Y. Belmabkhout, K. Adil, M. Eddaoudi, W. Koros, Conformation-controlled molecular sieving effects for membrane-based propylene/propane separation, Adv. Mater. 31 (2019) 1807513. https://doi.org/https://doi.org/10.1002/adma.201807513.

[22] J. Li, X. Han, X. Kang, Y. Chen, S. Xu, G.L. Smith, E. Tillotson, Y. Cheng, L.J. McCormick McPherson, S.J. Teat, S. Rudić, A.J. Ramirez-Cuesta, S.J. Haigh, M. Schröder, S. Yang, Purification of propylene and ethylene by a robust metal-organic framework mediated by host-guest interactions, Angew. Chem. Int. Ed. 60 (2021) 15541-15547. https://doi.org/https://doi.org/10.1002/anie.202103936.

[23] H.R. Amedi, M. Aghajani, Modified zeolitic-midazolate framework 8/poly(ether-block-amide) mixed-matrix membrane for propylene and propane separation, J. Appl. Polym. Sci. 135 (2018) 46273. https://doi.org/https://doi.org/10.1002/app.46273.

[24] S. Japip, H. Wang, Y. Xiao, T. Shung Chung, Highly permeable zeolitic imidazolate framework (ZIF)-71 nano-particles enhanced polyimide membranes for gas separation, J. Membr. Sci. 467 (2014) 162-174. https://doi.org/https://doi.org/10.1016/j.memsci.2014.05.025.

[25] M. Askari, T.-S. Chung, Natural gas purification and olefin/paraffin separation using thermal cross-linkable co-polyimide/ZIF-8 mixed matrix membranes, J. Membr. Sci. 444 (2013) 173-183. https://doi.org/https://doi.org/10.1016/j.memsci.2013.05.016.

[26] R. Lin, L. Ge, H. Diao, V. Rudolph, Z. Zhu, Propylene/propane selective mixed matrix membranes with grape-branched MOF/CNT filler, J. Mater. Chem. A 4 (2016) 6084-6090. https://doi.org/10.1039/C5TA10553F.

[27] H. An, S. Park, H.T. Kwon, H.-K. Jeong, J.S. Lee, A new superior competitor for exceptional propylene/propane separations: ZIF-67 containing mixed matrix membranes, J. Membr. Sci. 526 (2017) 367-376. https://doi.org/https://doi.org/10.1016/j.memsci.2016.12.053.

[28] H.R. Amedi, M. Aghajani, Poly urethane mixed matrix membranes for propylene and propane separation, Chem. Pap. 72 (2018) 1477-1485. https://doi.org/10.1007/s11696-018-0386-x.

[29] J. Yu, C. Wang, L. Xiang, Y. Xu, Y. Pan, Enhanced C_3H_6/C_3H_8 separation performance in poly(vinyl acetate) membrane blended with ZIF-8 nanocrystals, Chem. Eng. Sci. 179 (2018) 1-12. https://doi.org/https://doi.org/10.1016/j.ces.2017.12.051.

[30] S.H. Kunjattu, V. Ashok, A. Bhaskar, K. Pandare, R. Banerjee, U.K. Kharul, ZIF-8@DBzPBI-BuI composite membranes for olefin/paraffin separation, J. Membr. Sci. 549 (2018) 38-45. https://doi.org/https://doi.org/10.1016/j.memsci.2017.11.069.

[31] D. Liu, L. Xiang, H. Chang, K. Chen, C. Wang, Y. Pan, Y. Li, Z. Jiang, Rational matching between MOFs and polymers in mixed matrix membranes for propylene/propane separation, Chem. Eng. Sci. 204 (2019) 151-160. https://doi.org/https://doi.org/10.1016/j.ces.2019.04.032.

[32] F. Moghadam, T.H. Lee, I. Park, H.B. Park, Thermally annealed polyimide-based mixed matrix membrane containing ZIF-67 decorated porous graphene oxide nanosheets with enhanced propylene/propane selectivity, J. Membr. Sci. 603 (2020) 118019. https://doi.org/https://doi.org/10.1016/j.memsci.2020.118019.

[33] S. Park, H.-K. Jeong, In-situ linker doping as an effective means to tune zeolitic-imidazolate framework-8 (ZIF-8) fillers in mixed-matrix membranes for propylene/propane separation, J. Membr. Sci. 596 (2020) 117689. https://doi.org/https://doi.org/10.1016/j.memsci.2019.117689.

[34] J.W. Oh, K.Y. Cho, M.-Y. Kan, H.J. Yu, D.-Y. Kang, J.S. Lee, High-flux mixed matrix membranes containing bimetallic zeolitic imidazole framework-8 for C_3H_6/C_3H_8 separation, J. Membr. Sci. 596 (2020) 117735. https://doi.org/https://doi.org/10.1016/j.memsci.2019.117735.

[35] Y. Liu, H. Kita, K. Tanaka, K. Imawaka, S. Tanaka, T. Takewaki, Mechanochemically synthesized ZIF-8 nanoparticles blended into 6FDA-TrMPD membranes for C_3H_6/C_3H_8 separation, J. Appl. Polym. Sci. 138 (2021) e50251. https://doi.org/https://doi.org/10.1002/app.50251.

[36] W.S. Chi, S.J. Kim, S.-J. Lee, Y.-S. Bae, J.H. Kim, Enhanced performance of mixed-matrix membranes through a graft copolymer-directed interface and interaction tuning approach, ChemSusChem 8 (2015) 650-658. https://doi.org/https://doi.org/10.1002/cssc.201402677.

[37] Y. Su, D. Li, M. Shan, X. Feng, J. Gascon, Y. Wang, Y. Zhang, Uniformly distributed mixed matrix membranes via a solution processable strategy for propylene/propane separation, Angew. Chem. Int. Ed. 63 (2024) e202316093. https://doi.org/https://doi.org/10.1002/anie.202316093.

[38] O. Kwon, M. Kim, E. Choi, J.H. Bae, S. Yoo, J.C. Won, Y.H. Kim, J.H. Shin, J.S. Lee, D.W. Kim, High-aspect ratio zeolitic imidazolate framework (ZIF) nanoplates for hydrocarbon separation membranes, Sci. Adv. 8 (2022) eabl6841. https://doi.org/10.1126/sciadv.abl6841.

[39] D. Peng, X. Feng, G. Yang, X. Niu, Z. Liu, Y. Zhang, In-situ growth of silver complex on ZIF-8 towards mixed matrix membranes for propylene/propane separation, J. Membr. Sci. 668 (2023) 121267. https://doi.org/https://doi.org/10.1016/j.memsci.2022.121267.

[40] F. Hillman, M.R.A. Hamid, P. Krokidas, S. Moncho, E.N. Brothers, I.G. Economou, H.-K. Jeong, Delayed linker addition (DLA) synthesis for hybrid SOD ZIFs with unsubstituted imidazolate linkers for propylene/propane and n-Butane/i-Butane separations, Angew. Chem. Int. Ed. 60 (2021) 10103-10111. https://doi.org/https://doi.org/10.1002/anie.202015635.

[41] S. Li, X. Shangguan, Z. Zhou, W. Niu, Y. Zhang, X. Wang, H. Zhu, G. Liu, K. Wang, G. Yu, Immobilization of ferrocene and its derivatives within metal-organic frameworks with high loadings toward efficient oxygen evolution reaction, Dalton Trans. 53 (2024) 1568-1574. https://doi.org/10.1039/D3DT02763E.

[42] L. Wang, Y. Cao, M. Zhou, S.J. Zhou, Q. Yuan, Novel copolyimide membranes for gas separation, J. Membr. Sci. 305 (2007) 338-346. https://doi.org/https://doi.org/10.1016/j.memsci.2007.08.024.

[43] H. Jiang, Y. Chen, S. Song, Z. Guo, Z. Zhang, C. Zheng, G. He, H. Wang, H. Wu, T. Huang, Y. Ren, X. Liu, J. Zhang, Y. Yin, Z. Jiang, M.D. Guiver, Confined facilitated transport within covalent organic frameworks for propylene/propane membrane separation, Chem. Eng. J. 439 (2022) 135657. https://doi.org/https://doi.org/10.1016/j.cej.2022.135657.

[44] K.S. Park, Z. Ni, A.P. Côté, J.Y. Choi, R. Huang, F.J. Uribe-Romo, H.K. Chae, M. O'Keeffe, O.M. Yaghi, Exceptional chemical and thermal stability of zeolitic imidazolate frameworks, Proc. Natl. Acad. Sci. 103 (2006) 10186-10191. https://doi.org/10.1073/pnas.0602439103.

[45] K. Li, M. Chen, L. Chen, S. Zhao, W. Pan, P. Li, Y. Han, Adsorption of tetracycline from aqueous solution by ZIF-8: Isotherms, kinetics and thermodynamics, Environ. Res. 241 (2024) 117588. https://doi.org/https://doi.org/10.1016/j.envres.2023.117588.

[46] K.M. Ok, J. Sung, G. Hu, R.M.J. Jacobs, D. O'Hare, TOF-2: a large 1D channel thorium organic framework, J. Am. Chem. Soc. 130 (2008) 3762-3763. https://doi.org/10.1021/ja800395q.

[47] T.K. Maji, R. Matsuda, S. Kitagawa, A flexible interpenetrating coordination framework with a bimodal porous functionality, Nat. Mater. 6 (2007) 142-148. https://doi.org/10.1038/nmat1827.

[48] Z. Wang, W. Wang, T. Zeng, D. Ma, P. Zhang, S. Zhao, L. Yang, X. Zou, G.

Zhu, Covalent-linking-enabled superior compatibility of ZIF-8 hybrid membrane for efficient propylene separation, Adv. Mater. 34 (2022) 2104606. https://doi.org/10.1002/adma.202104606.

[49] Q. Ding, S. Zhang, Recent advances in the development of metal-organic frameworks for propylene and propane separation, Energy Fuels 36 (2022) 7337-7361. https://doi.org/10.1021/acs.energyfuels.2c01427.

[50] P. Hu, J. Han, J. Zhou, H. Wang, C. Xiong, H. Liu, X. Zhou, Y. Wang, H. Ji, Customized H-bonding acceptor and aperture chemistry within a metal-organic framework for efficient C_3H_6/C_3H_8 separation, Chem. Eng. J. 426 (2021) 131302. https://doi.org/https://doi.org/10.1016/j.cej.2021.131302.

[51] N. Lamia, M. Jorge, M.A. Granato, F.A. Almeida Paz, H. Chevreau, A.E. Rodrigues, Adsorption of propane, propylene and isobutane on a metal-organic framework: molecular simulation and experiment, Chem. Eng. Sci. 64 (2009) 3246-3259. https://doi.org/https://doi.org/10.1016/j.ces.2009.04.010.

[52] E.D. Bloch, W.L. Queen, R. Krishna, J.M. Zadrozny, C.M. Brown, J.R. Long, Hydrocarbon separations in a metal-organic framework with open iron(II) coordination sites, Science 335 (2012) 1606-1610. https://doi.org/10.1126/science.1217544.

[53] Z. Zhang, Q. Ding, X. Cui, X.-M. Jiang, H. Xing, Fine-tuning and selective-binding within an anion-functionalized ultramicroporous metal-organic framework for efficient olefin/paraffin separation, ACS Appl. Mater. Interfaces 12 (2020) 40229-40235. https://doi.org/10.1021/acsami.0c07800.

[54] G. Yu, Y. Li, Z. Wang, T.X. Liu, G. Zhu, X. Zou, Mixed matrix membranes derived from nanoscale porous organic frameworks for permeable and selective CO_2 separation, J. Membr. Sci. 591 (2019) 117343. https://doi.org/https://doi.org/10.1016/j.memsci.2019.117343.

[55] Y. Cheng, B. Joarder, S.J. Datta, N. Alsadun, D. Poloneeva, D. Fan, R. Khairova, A. Bavykina, J. Jia, O. Shekhah, A. Shkurenko, G. Maurin, J. Gascon, M. Eddaoudi, Mixed matrix membranes with surface functionalized metal-organic framework sieves for efficient propylene/propane separation, Adv. Mater. 35 (2023) 2300296. https://doi.org/https://doi.org/10.1002/adma.202300296.

[56] L.C. Tomé, D.C. Guerreiro, R.M. Teodoro, V.D. Alves, I.M. Marrucho, Effect of polymer molecular weight on the physical properties and CO_2/N_2 separation of pyrrolidinium-based poly(ionic liquid) membranes, J. Membr. Sci. 549 (2018) 267-274. https://doi.org/10.1016/j.memsci.2017.12.019.

[57] A. Oxley, A.G. Livingston, Effect of polymer molecular weight on the long-term process stability of crosslinked polybenzimidazole organic solvent nanofiltration

(OSN) membranes, J. Membr. Sci. 689 (2024) 122149. https://doi.org/10.1016/j.memsci.2023.122149.

[58] I. Soroko, M. Sairam, A.G. Livingston, The effect of membrane formation parameters on performance of polyimide membranes for organic solvent nanofiltration (OSN). Part C. Effect of polyimide characteristics, J. Membr. Sci. 381 (2011) 172-182. https://doi.org/10.1016/j.memsci.2011.07.029.

[59] H. Jin, Z. Wang, G. Yu, J. Dong, S. Zhao, F. Cui, H. Zhang, G. Lu, X. Zou, Z. Chang, A customized zeolitic imidazolate framework enabling bionic preconcentration of ultralow CO_2, Sci. China Mater. 67 (2024) 3401-3407. https://doi.org/10.1007/s40843-024-3044-0.

[60] Y. Chen, H. Wu, L. Yu, S. Tu, Y. Wu, Z. Li, Q. Xia, Separation of propylene and propane with pillar-layer metal-organic frameworks by exploiting thermodynamic-kinetic synergetic effect, Chem. Eng. J. 431 (2022) 133284. https://doi.org/10.1016/j.cej.2021.133284.

[61] D. Nobakht, R. Abedini, A new ternary Pebax®1657/maltitol/ZIF-8 mixed matrix membrane for efficient CO_2 separation, Process Saf. Environ. Prot. 170 (2023), 709-719. https://doi.org/10.1016/j.psep.2022.12.058.

[62] B. Zornoza, A. Martinez-Joaristi, P. Serra-Crespo, C. Tellez, J. Coronas, J. Gascon, F. Kapteijn, Functionalized flexible MOFs as fillers in mixed matrix membranes for highly selective separation of CO_2 from CH_4 at elevated pressures, Chem. Commun. 47 (2011) 9522-9524. https://doi.org/10.1039/C1CC13431K.

[63] R. Abedini, M. Omidkhah, F. Dorosti, Hydrogen separation and purification with poly (4-methyl-1-pentyne)/MIL 53 mixed matrix membrane based on reverse selectivity, Int. J. Hydrogen Energy 39 (2014) 7897-7909. https://doi.org/10.1016/j.ijhydene.2014.03.027.

Highlights:

· A porous MOF of CN-ZIF-8 was synthesized with uncoordinated cyano groups.

· Continuous mixed-matrix membranes of CN-ZIF-8/6FDA-DAM were successfully prepared for C_3H_6/C_3H_8 separation.

· The separation performances greatly surpassed the trade-off plot.

· The synergy of thermodynamic and kinetic effects was clarified.